NANO LETTERS

2009
Vol. 9, No. 9
3203-3208

Quantifying the Semiconducting Fraction in Single-Walled Carbon Nanotube Samples through Comparative Atomic Force and Photoluminescence Microscopies

Anton V. Naumov,[†] Oleg A. Kuznetsov,[§] Avetik R. Harutyunyan,[§] Alexander A. Green,[||] Mark C. Hersam,[||] Daniel E. Resasco,[⊥] Pavel N. Nikolaev,[#] and R. Bruce Weisman*,[‡]

Applied Physics Program, Department of Chemistry, and Richard E. Smalley Institute for Nanoscale Science and Technology, Rice University, 6100 Main Street, Houston, Texas 77005, Honda Research Institute USA, Inc., 1381 Kinnear Road, Columbus, Ohio 43212, Department of Materials Science and Engineering, Department of Chemistry, Northwestern University, 2220 Campus Drive, Evanston, Illinois 60208, School of Chemical, Biological, and Materials Engineering, University of Oklahoma, 100 East Boyd Street, Norman, Oklahoma 73019, and ERC Inc./NASA-Johnson Space Center, Houston, Texas 77058

Received May 5, 2009; Revised Manuscript Received July 3, 2009

ABSTRACT

A new method was used to measure the fraction of semiconducting nanotubes in various as-grown or processed single-walled carbon nanotube (SWCNT) samples. SWCNT number densities were compared in images from near-IR photoluminescence (semiconducting species) and AFM (all species) to compute the semiconducting fraction. The results show large variations among growth methods and effective sorting by density gradient ultracentrifugation. This counting-based method provides important information about SWCNT sample compositions that can guide controlled growth methods and help calibrate bulk characterization techniques.

Single-walled carbon nanotubes (SWCNTs) remain the subject of intense research. Much of this interest arises from the diversity of their electronic properties, which include both semiconducting and metallic structural forms.[1] In a number of possible applications, including the use of SWCNTs as field emission sources,[2] nanoscale electrical interconnects,[3] field-effect transistors,[4−6] and conductive transparent films,[7,8] it is desirable to use nanotubes of only a single electronic type. It is expected that such selected samples can be obtained through controlled growth combined with subsequent purification techniques.

Several methods can be used to produce SWCNTs. The first to be reported was the arc discharge graphite evaporation method that allowed Iijima et al. to discover these materials.[9] Another growth method uses laser ablation of graphite targets at high temperatures.[10] At present, the most widespread method is chemical vapor deposition (CVD) in which decomposition of carbon-rich gases on a catalytic substrate yields carbon nanostructures. The first production of SWCNTs by CVD was reported by Dai et al.[11] Further developments of this technique evolved into the HiPco (high pressure carbon monoxide) and CoMoCAT growth processes.[12,13] In the HiPco method, carbon nanotubes are produced by catalytic disproportionation of carbon monoxide gas at high temperatures and pressures. In the CoMoCAT process, disproportionation of carbon monoxide occurs on a SiO_2-supported Co−Mo catalyst at lower pressures and temperatures as compared to HiPco.[13,14] Lower temperature syntheses and stabilization of small cobalt metal clusters by interaction with molybdenum yield CoMoCAT product with

* To whom correspondence should be addressed. E-mail:weisman@rice.edu.
[†] Applied Physics Program, Rice University.
[‡] Department of Chemistry, and Richard E. Smalley Institute for Nanoscale Science and Technology, Rice University.
[§] Honda Research Institute USA, Inc.
[||] Northwestern University.
[⊥] University of Oklahoma.
[#] ERC Inc./NASA-Johnson Space Center.

10.1021/nl9014342 CCC: $40.75
Published on Web 07/29/2009

smaller average diameter and a narrower distribution of structures compared to those synthesized at higher temperatures.[15] Although the most refined current growth methods are significantly selective for nanotube structure and electronic type, many applications require samples that are more highly sorted. For this purpose, several postgrowth processing methods have been developed.[16−21] One of the most effective of these is density gradient ultracentrifugation (DGU),[22−24] which can physically sort carbon nanotubes by chirality or electronic type through ultracentrifugation of SWCNT suspensions in a density gradient.

Reliable characterization is a key step in the preparation of pure semiconducting or metallic SWCNT samples. At the level of individual nanotubes, the two types can be distinguished and counted by specific (*n,m*) determination through highly resolved scanning tunneling microscopy (STM)[25] or electron nanodiffraction.[26,27] However, these precise microscopic methods are too tedious for routine use. The metallic/semiconducting composition of a sample can also in principle be determined by counting individual nanotubes using voltage-contrast SEM, which distinguishes metallic from semiconducting SWCNTs.[28] We note that this approach involves the complexity of size exclusion chromatography followed by electrophoretic SWCNT deposition. In addition, systematic errors may arise from nonuniform sampling or the presence of small bundles of mixed electronic type. Recently, electric force scanning probe microscopy has been applied to recognize and count individual metallic and semiconducting SWCNTs longer than 200 nm and determine sample compositions.[29] Another counting-based method is direct charge transport or electrical breakdown measurements on SWCNT field-effect transistors to classify nanotubes as metallic or semiconducting.[30,31] The laborious nature of this approach makes it difficult to achieve high statistical accuracy, and results may also be influenced by clustering and sampling inefficiency. Photoluminescence (PL) spectroscopy offers an incisive probe of bulk or individual semiconducting SWCNTs,[32−34] but does not detect metallic species. Raman spectroscopy also provides a relatively rapid tool for studying SWCNTs as individuals or bulk ensembles.[35,36] However, it has the disadvantage of requiring a wide variety of incident laser wavelengths to detect nanotubes spanning a range of structures. Raman has been used to estimate the relative semiconducting and metallic contents in processed SWCNT samples,[17,37,38] but the calibration factors needed to extract reliable values of these ratios are not known. Visible-near-IR absorption spectroscopy of SWCNT samples reveals distinct optical transitions of semiconducting and metallic species[19,39] and appears more promising for quantitative determination of metallic/semiconducting ratios if adequate and consistent calibration methods become available. Recent reports show progress in this area,[30,40,41] but some challenges may remain in accurately subtracting background absorptions and acquiring well-characterized reference samples.

We report here a new counting-based method for the absolute measurement of semiconducting fractions in SWCNT samples. In this approach, we capture AFM and near-IR photoluminescence images of dried dilute SWCNT dispersions. Both semiconducting and metallic species are visible in the AFM images, while only semiconducting nanotubes are visible in photoluminescence. The ratio of observed nanotube densities therefore gives the semiconducting fraction in the sample. We have performed this analysis on SWCNTs prepared by a variety of growth and/or postprocessing methods. The results provide compositional reference data that should be useful to researchers working with such samples or attempting to calibrate bulk analysis techniques.

Several SWCNT batches produced by different methods were analyzed in this work. These included raw product made by the HiPco method at Rice University (batch 166.12), by a CVD process at the Honda Research Institute USA Inc. (Columbus, Ohio), by laser ablation at NASA-Johnson Space Center, and by the University of Oklahoma CoMoCAT method at SouthWest Nanotechnologies Inc. The CoMoCAT sample was purified and freeze-dried before analysis. We also analyzed SWCNTs that had been processed by density gradient separation at Northwestern University starting from raw HiPco SWCNTs (Carbon Nanotechnologies, Inc., batch R0559). Judging by the diameter distributions deduced from AFM image analysis (see Supporting Information, Figure S1), the photoluminescence emission of each of these SWCNT samples was predicted to fall within the spectral range of our InGaAs detector. Raw SWCNT samples were initially bath sonicated for 3 h in 1% aqueous sodium dodecyl sulfate (SDS) solutions to give concentrated SWCNT suspensions. The suspensions were then centrifuged at 26700 × g for 6 h. To avoid excessive losses, the smaller CVD and laser ablation samples were instead centrifuged at 14500 × g for 10 to 30 min in a table-top centrifuge. After centrifuging, the pellets were discarded and the supernatants were diluted by factors of 14−24 to adjust SWCNT and SDS concentrations to convenient levels. These diluted suspensions were then tip-sonicated for 2 min at 5−7 W to disaggregate residual SWCNT bundles before spin-coating onto polished fused silica slides. These slides had previously been spin coated with 0.05% aqueous SDS solution, rinsed with deionized water, and annealed for 30 min in air at 550 °C to obtain clean and flat surfaces. The sample preparation procedure for density gradient sorted SWCNTs was quite different. Those SWCNTs were extracted from the density gradient in solutions containing SDS, sodium cholate, and iodixanol[24] and concentrated in step density gradients. To prevent uneven AFM backgrounds arising from sodium cholate and iodixanol aggregates, the samples were dialyzed against 1% w/v SDS aqueous solution for 49 h using 20k molecular-weight cutoff dialysis cassettes (Pierce Chemical), which removed the sodium cholate and iodixanol from solution. The dialyzed solutions were diluted by factors of 14−24 and subjected to intense bath sonication (Sharpertek ultrasonic cleaner). The resulting suspensions were then tip-sonicated for 30 s at 5 W and spin-coated onto 15 × 15 × 0.15 mm mica slides.

After the slides were coated with aqueous surfactant suspensions of SWCNTs, the total number of SWCNTs per unit area was determined from AFM images, and the number of semiconducting SWCNTs per unit area was found from

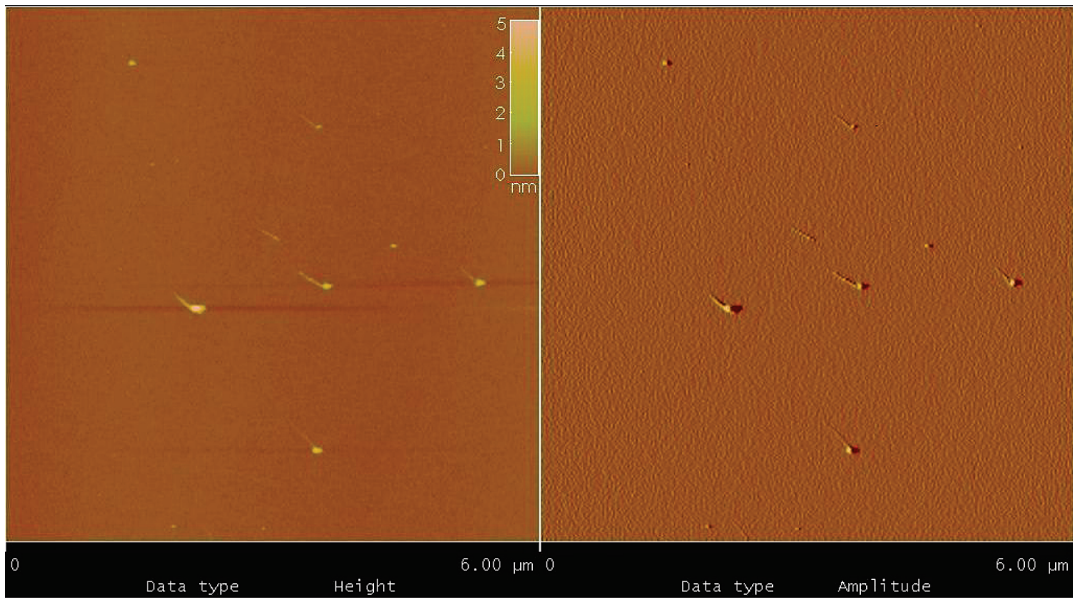

Figure 1. Tapping mode AFM images of individual SWCNTs from a DGU-processed semiconducting enriched sample in dried SDS on a cleaved mica surface. Amplitude image is shown in the right panel; height is shown in the left panel. Each panel shows a 6 × 6 μm region.

near-IR photoluminescence images. A Veeco AFM (Multimode 3A) was used to study up to 40 regions, each 10 × 10 μm or 6 × 6 μm, within a ~100 × 100 μm area of the sample. The number of SWCNTs in each image was counted (Figure 1). Photoluminescence of individual semiconducting SWCNTs in the sample was observed using a custom built near-IR fluorescence microscope.[34] In this setup, semiconducting SWCNTs were excited in their E_{22} transitions with 660 and 780 nm diode lasers. Our experience in photoluminescence analysis indicates that this combination of excitation wavelengths will induce detectable emission from essentially all semiconducting (n,m) species in the studied samples. This occurs because of the high detection sensitivity and the large effective resonance windows arising from long Lorentzian tails of the principal E_{22} peaks, plus many weaker spectral features from E_{22} vibronic sidebands, E_{11} vibronic sidebands, higher excitonic bands associated with E_{22}, and underlying continuum-like transitions. Near-IR E_{11} photoluminescence emission was collected through the quartz substrate by a Nikon Plan Apo 60×, NA = 1 water immersion objective on a Nikon TE-2000U inverted microscope. Fluorescence of SWCNTs on mica substrates was instead collected directly with a Nikon CF Plan 100×, NA = 0.95 air objective. The microscope was coupled through a 946 nm long-pass filter to a liquid nitrogen-cooled Roper OMA V 2D InGaAs camera to image NIR emission from semiconducting SWCNTs on the sample surface (Figure 2). To monitor emission spectra of individual SWCNTs, the emitted light from a small region of the image plane could be directed into a spectrograph and detected by a 512-channel InGaAs linear array. For each sample, numerous regions of 10 × 10 μm or 6 × 6 μm (depending on the magnification of the objective) were examined (see Supporting Information Table S1) to find the number of semiconducting SWCNTs per unit area. Then the semiconducting fraction in each sample was found as the average of the ratio of the number of semiconducting SWCNTs per unit area to the total number of SWCNTs per unit area.

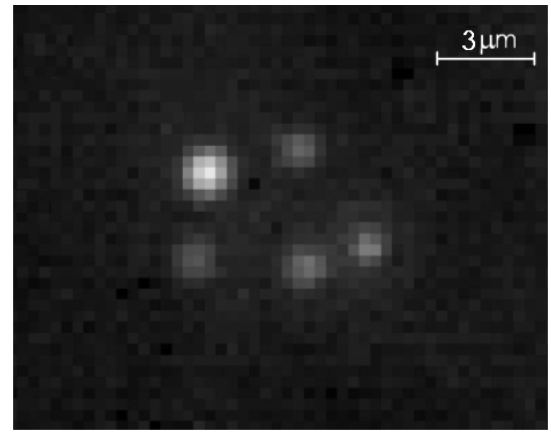

Figure 2. Near-IR photoluminescence image of individual SWCNTs from the same DGU-processed semiconducting enriched sample in dried SDS on a cleaved mica surface.

In our experiments only individual, disaggregated SWCNTs were counted. During AFM imaging, the few residual bundles were identified on the basis of height profiling and omitted from the counts. (See Supporting Information Figure S1 for height criteria.) As seen from Figure 1, the number of SWCNTs per 6 × 6 μm region could be easily determined and their diameters estimated from height profile analysis. Individual SWCNTs commonly showed height variations along their lengths attributed to regions of irregular surfactant coating. The minimum profile heights for SWCNTs in Figure 1 ranged from 0.7 to 1.35 nm, consistent with the diameter distribution of SWCNTs in our samples and smaller than would be expected for bundled nanotubes.

Photoluminescence images have far coarser spatial resolution than AFM images, and may therefore not distinguish individual nanotubes from bundles or loose aggregates. To

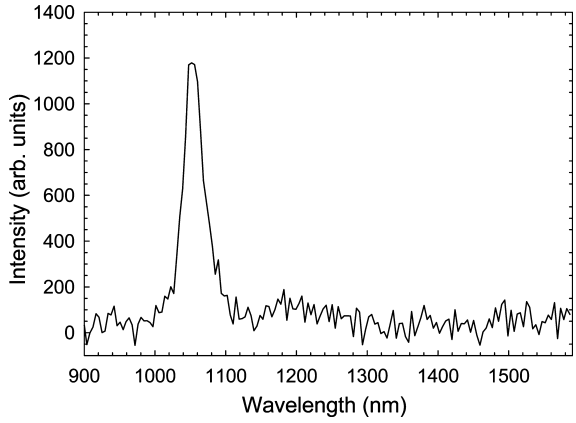

Figure 3. Near-IR photoluminescence spectrum of a single SWCNT in dried SDS on a fused silica substrate.

avoid counting loose aggregates, we examined the emission spectra of objects that appeared not to be point emitters and excluded them if their spectra were broader or more complex than expected for an individual SWCNT (see Figure 3 for a normal emission spectrum). Bundles in samples containing significant metallic content are likely to be nonemissive, and therefore uncounted, because of efficient energy transfer to a metallic tube.[42] However, there is the possibility that our method may count small semiconducting bundles in photoluminescence that were recognized and not counted in AFM. We note that the fraction of nanotube objects appearing to be bundles in AFM images ranged from 5 to 15% (Supporting Information, Figure S1) with semiconducting-rich samples falling near the bottom of this range and thus presenting only a minor chance for semiconducting bundle miscounting. Another possible source of error is the finite sensitivity of PL detection. This could cause undercounting of unbundled semiconducting SWCNTs that emit very weakly because of defects or surface functionalization, leading to a negative error in the deduced semiconducting fraction. To minimize such errors, we used increased excitation intensities and integration times to distinguish weak emitters from background noise. We estimate that this method let us count imperfect SWCNTs unless they were so damaged as to contain no electronically intact segments longer than ~100 nm. Under the processing conditions used here, we expect that only a negligible fraction of nanotubes sustained such extensive damage. SWCNTs that are ultrasonically cut to lengths below 100 nm might also escape PL detection, but AFM data show that the vast majority of SWCNTs in our samples have lengths between 200 and 700 nm.

Another possible error source arises from the fact that we do not image exactly the same sample regions in AFM and photoluminescence. Because each measured small region contains only a few nanotubes, there would be a large statistical error in the ratio found for each region even with perfect registration between images. By counting in many distinct but nonregistered small regions and then adding the counts, we obtain a ratio that approaches the (true) limit that would be found by counting nanotubes over the entire sample using both AFM and PL. For every sample batch we typically examined at least 40 different regions, each 10×10 μm or 6×6 μm, to give nanotube counts exceeding 200 for each method. The combined number of SWCNTs counted in this work exceeds 12000 (see Table S1 in Supporting Information). Measurements for each sample batch were performed on three or more spin-coated replicates. Table 1 shows the semiconducting percentages computed by averaging these replicate determinations and the standard errors of the mean percentages. We estimate that our results have uncertainties ranging from 0.5 to 4%.

The findings in Table 1 generally seem consistent with expectations based on the growth and processing methods used to prepare the samples. For example, HiPco SWCNTs are known to grow in a wide variety of (n,m) structures and are presumed to comprise a nearly statistical distribution of two-thirds semiconducting and one-third metallic nanotubes. Our results (Table 1) show a HiPco semiconducting content within 4% of that expected value. The standard grade CoMoCAT SWCNTs produced by a lower temperature process are known to contain high concentrations of the semiconducting (6,5) and (7,6) species[43] and may have a metallic content below the 33% statistical value. Our findings confirm a high semiconducting fraction of 92.1% in a standard grade CoMoCAT sample. It has been proposed that for small diameter nanotubes the formation of caps leading to zigzag nanotubes is thermodynamically and kinetically unfavorable.[44] Likewise, it is believed that the preference for semiconducting near-armchair structures in CoMoCAT samples arises from a combination of the stability of the nanotube cap on a catalyst surface and the activation energy for carbon atom incorporation into the nanotube during growth. The caps for armchair nanotubes are stable, but for that reason also give higher activation energies for carbon incorporation and therefore decreased production of these metallic armchair species at low temperatures. By comparison, the growth interfaces of near-armchair species (e.g., (6,5), (7,6), etc.) are somewhat less stable and allow carbon incorporation with a lower activation energy. These differences among activation energies are expected to be greatest in the small-diameter region, narrowing the distribution of chiralities in samples synthesized at low temperatures

Table 1. Compositions Determined for As-Produced or Processed SWCNT Samples

sample	source	% semiconducting	% metallic	% standard error
HiPco	Rice Univ.	62.9	37.1	0.5
CoMoCAT, standard grade	SWeNT Inc.	92.1	7.9	1.1
CoMoCAT, commercial grade	SWeNT Inc.	51.9	48.1	3.5
laser ablation, low temperature method	ERC Inc./NASA-JSC	54.7	45.3	1.4
CVD preferential growth	Honda Res. Inst. USA Inc.	15.4	84.6	2.6
HiPco, starting material	Northwestern Univ.	60.5	39.5	3.8
HiPco, semiconducting-enriched by DGU	Northwestern Univ.	96.0	4.0	0.6
HiPco, metallic-enriched by DGU	Northwestern Univ.	3.1	96.9	0.6

compared to those synthesized at high temperatures.[45] Accordingly, the commercial grade CoMoCAT sample, produced at higher temperatures, includes a broader range of species and is found here to contain only 52% semiconducting SWCNTs.

It is also possible to tune a CVD growth process for even higher metallic contents. This is illustrated by samples from Honda Research Institute USA Inc., which were grown via methane decomposition on Fe nanocatalysts that were previously annealed in situ under inert gas ambient in the presence of oxidative species. We find this product to contain 15% semiconducting, and therefore 85% metallic SWCNTs. This is the lowest semiconducting fraction found among the samples that had not undergone postgrowth separation treatments. It is also far lower than the semiconducting fractions found in the other CVD samples analyzed here. Our analysis is consistent with an independent estimate of the semiconducting content obtained by analyzing ratios of integrated Raman radial breathing mode intensities (with 632.8 nm excitation) and comparing to a HiPco standard,[46] analogous to the method used by Krupke, et al.

In addition to HiPco and CVD grown SWCNTs, we have also analyzed laser ablation samples grown at the NASA-Johnson Space Center.[47−50] These SWCNTs were produced at 900 °C (as opposed to the more common 1200 °C) in order to reduce the average diameter and bring E_{11} transitions into the detection range of the spectrometer.[51] In this laser ablation sample, we found 55% semiconducting nanotubes.

In order to further test our method and characterize the semiconducting fraction in SWCNT samples processed by density gradient ultracentrifugation (DGU), we have analyzed samples prepared at Northwestern University. These consisted of fractionated HiPco nanotubes enriched in semiconducting or metallic species. We determined the semiconducting content of the starting material as well as of the enriched samples. As expected, the starting material was found to have a semiconducting content within 2.5% of the value determined separately for HiPco SWCNTs (Table 1). However, the metallic and semiconducting enriched samples differed dramatically from the starting material, with semiconducting fractions of 2.6 and 96%, respectively (Table 1). These results confirm highly selective electronic type sorting through the DGU processing and are consistent with purity estimates based on optical absorbance data.[24]

In summary, we have demonstrated a new counting-based method for measuring the semiconducting fraction in SWCNT samples. This method was applied to analyze a variety of SWCNT batches produced by different growth techniques or purified by DGU. Our results, based on measurements of hundreds of nanotubes per sample, show good precision and appear consistent with prior expectations for the sample compositions. The findings can serve as a useful reference for researchers growing or using SWCNTs prepared by these methods. They may also assist in the absolute calibration of bulk spectroscopic characterization methods.

Acknowledgment. This research was supported at Rice University by grants from the National Science Foundation (CHE-0809020) and the Welch Foundation (C-0807); at Northwestern University by a Natural Sciences and Engineering Research Council of Canada Postgraduate Scholarship (A.A.G.) and grants from the National Science Foundation (DMR-0520513, EEC-0647560, and DMR-0706067); at Honda Research Institute USA Inc. by an internship grant; at NASA by contract no. NNJ05HI05C and support from the State of Texas, Space Act Agreement no. SAA-AT-07-021 (RAN 0798) (UTA07-099); and at the University of Oklahoma by the Department of Energy - Basic Energy Sciences (Grants DEFG03-02ER15345 and DE-FG02-06ER64239).

Supporting Information Available: SWCNT height distribution found from AFM measurements, and more detailed statistical data related to SWCNT semiconducting fraction determination. This material is available free of charge via the Internet at http://pubs.acs.org.

References

(1) Saito, R.; Dresselhaus, G.; Dresselhaus, M. S. *Physical Properties of Carbon Nanotubes*; Imperial College Press: London, 1998.
(2) Lim, S. C.; Lee, K.; Lee, I. H.; Lee, Y. H. *Nano* **2007**, *2*, 69–89.
(3) Yao, Z.; Kane, C. L.; Dekker, C. *Phys. Rev. Lett.* **2000**, *84*, 2941–2944.
(4) Avouris, P.; Radosavljevic, M.; Wind, S. J. Carbon Nanotube Electronics and Optoelectronics. In *Applied Physics of Carbon Nanotubes*; Rotkin, S. V., Subramoney, S., Eds.; Springer: Berlin, 2005; pp 227−251.
(5) Martel, R.; Schmidt, T.; Shea, H. R.; Hertel, T.; Avouris, P. *Appl. Phys. Lett.* **1998**, *73*, 2447–2449.
(6) Tans, S. J.; Verschueren, A. R. M.; Dekker, C. *Nature* **1998**, *393*, 49–52.
(7) Wu, Z. C.; Chen, Z. H.; Du, X.; Logan, J. M.; Sippel, J.; Nikolou, M.; Kamaras, K.; Reynolds, J. R.; Tanner, D. B.; Hebard, A. F.; Rinzler, A. G. *Science* **2004**, *305*, 1273–1276.
(8) Yu, X.; Rajamani, R.; Stelson, K. A.; Cui, T. *J. Nanosci. Nanotechnol.* **2006**, *6*, 1939–1944.
(9) Iijima, S.; Ichihashi, T. *Nature* **1993**, *363*, 603–605.
(10) Thess, A.; Lee, R.; Nikolaev, P.; Dai, H.; Petit, P.; Robert, J.; Xu, C.; Lee, Y. H.; Kim, S. G.; Rinzler, A. G.; Colbert, D. T.; Scuseria, G. E.; Tomanek, D.; Fischer, J. E.; Smalley, R. E. *Science* **1996**, *273*, 483–487.
(11) Dai, H. J.; Rinzler, A. G.; Nikolaev, P.; Thess, A.; Colbert, D. T.; Smalley, R. E. *Chem. Phys. Lett.* **1996**, *260*, 471–475.
(12) Nikolaev, P.; Bronikowski, M. J.; Bradley, R. K.; Rohmund, F.; Colbert, D. T.; Smith, K. A.; Smalley, R. E. *Chem. Phys. Lett.* **1999**, *313*, 91–97.
(13) Kitiyanan, B.; Alvarez, W. E.; Harwell, J. H.; Resasco, D. E. *Chem. Phys. Lett.* **2000**, *317*, 497–503.
(14) Alvarez, W. E.; Pompeo, F.; Herrera, J. E.; Balzano, L.; Resasco, D. E. *Chem. Mater.* **2002**, *14*, 1853–1858.
(15) Resasco, D. E.; Alvarez, W. E.; Pompeo, F.; Balzano, L.; Herrera, J. E.; Kitiyanan, B.; Borgna, A. *J. Nanopart. Res.* **2002**, *4*, 131–136.
(16) Zheng, M.; Jagota, A.; Semke, E. D.; Diner, B. A.; McClean, R. S.; Lustig, S. R.; Richardson, R. E.; Tassi, N. G. *Nat. Mater.* **2003**, *2*, 338–342.
(17) Zheng, M.; Jagota, A.; Strano, M. S.; Santos, A. P.; Barone, P. W.; Chou, S. G.; Diner, B. A.; Dresselhaus, M. S.; McIean, R. S.; Onoa, G. B.; Samsonidze, G. G.; Semke, E. D.; Usrey, M. L.; Walls, D. J. *Science* **2003**, *302*, 1545–1548.
(18) Zheng, M.; Semke, E. D. *J. Am. Chem. Soc.* **2007**, *129*, 6084–6085.
(19) Chen, Z. H.; Du, X.; Du, M. H.; Rancken, C. D.; Cheng, H. P.; Rinzler, A. G. *Nano Lett.* **2003**, *3*, 1245–1249.
(20) Krupke, R.; Hennrich, F.; Kappes, M. M.; Lohneysen, H. V. *Nano Lett.* **2004**, *4*, 1395–1399.
(21) Hersam, M. C. *Nat. Nanotechnol.* **2008**, *3*, 387–394.
(22) Arnold, M. S.; Stupp, S. I.; Hersam, M. C. *Nano Lett.* **2005**, *5*, 713–718.
(23) Arnold, M. S.; Green, A. A.; Hulvat, J. F.; Stupp, S. I.; Hersam, M. C. *Nat. Nanotechnol.* **2006**, *1*, 60–65.
(24) Green, A. A.; Hersam, M. C. *Nano Lett.* **2008**, *8*, 1417–1422.

(25) Wildoer, J. W. G.; Venema, L. C.; Rinzler, A. G.; Smalley, R. E.; Dekker, C. *Nature* **1998**, *391*, 59–62.
(26) Qin, L.-C.; Iijima, S.; Kataura, H.; Maniwa, Y.; Suzuki, S.; Achiba, Y. *Chem. Phys. Lett.* **1997**, *268*, 101–106.
(27) Gao, M.; Zuo, J. M.; Twesten, R. D.; Petrov, I. *Appl. Phys. Lett.* **2003**, *82*, 2703–2705.
(28) Vijayaraghavan, A.; Blatt, S.; Marquardt, C.; Dehm, S.; Wahi, R.; Hennrich, F.; Krupke, R. *Nano Res.* **2009**, *1*, 321–332.
(29) Lu, W.; Xiong, Y.; Hassanien, A.; Zhao, W.; Zheng, M.; Chen, L. *Nano Lett.* **2009**, *9*, 1668–1672.
(30) Kim, W. J.; Lee, C. Y.; O'brien, K. P.; Plombon, J. J.; Blackwell, J. M.; Strano, M. S. *J. Am. Chem. Soc.* **2009**, *131*, 3128–3129.
(31) Li, Y. M.; Mann, D.; Rolandi, M.; Kim, W.; Ural, A.; Hung, S.; Javey, A.; Cao, J.; Wang, D. W.; Yenilmez, E.; Wang, Q.; Gibbons, J. F.; Nishi, Y.; Dai, H. J. *Nano Lett.* **2004**, *4*, 317–321.
(32) Bachilo, S. M.; Strano, M. S.; Kittrell, C.; Hauge, R. H.; Smalley, R. E.; Weisman, R. B. *Science* **2002**, *298*, 2361–2366.
(33) Weisman, R. B.; Bachilo, S. M. *Nano Lett.* **2003**, *3*, 1235–1238.
(34) Tsyboulski, D. A.; Bachilo, S. M.; Weisman, R. B. *Nano Lett.* **2005**, *5*, 975–979.
(35) Jorio, A.; Saito, R.; Hafner, J. H.; Lieber, C. M.; Hunter, M.; McClure, T.; Dresselhaus, G.; Dresselhaus, M. S. *Phys. Rev. Lett.* **2001**, *86*, 1118–1121.
(36) Rao, A. M.; Richter, E.; Bandow, S.; Chase, B.; Eklund, P. C.; Williams, K. A.; Fang, S.; Subbaswamy, K. R.; Menon, M.; Thess, A.; Smalley, R. E.; Dresselhaus, G.; Dresselhaus, M. S. *Science* **1997**, *275*, 187–191.
(37) Strano, M. S.; Dyke, C. A.; Usrey, M. L.; Barone, P. W.; Allen, M. J.; Shan, H. W.; Kittrell, C.; Hauge, R. H.; Tour, J. M.; Smalley, R. E. *Science* **2003**, *301*, 1519–1522.
(38) Krupke, R.; Hennrich, F.; von Lohneysen, H.; Kappes, M. M. *Science* **2003**, *301*, 344–347.
(39) Kataura, H.; Kumazawa, Y.; Maniwa, Y.; Umezu, I.; Suzuki, S.; Ohtsuka, Y.; Achiba, Y. *Synth. Met.* **1999**, *103*, 2555–2558.
(40) Miyata, Y.; Yanagi, K.; Maniwa, Y.; Kataura, H. *J. Phys. Chem. C* **2008**, *112*, 13187–13191.
(41) Blackburn, J. L.; Barnes, T. M.; Beard, M. C.; Kim, Y. H.; Tenent, R. C.; McDonald, T. J.; To, B.; Coutts, T. J.; Heben, M. J. *ACS Nano* **2008**, *2*, 1266–1274.
(42) O'Connell, M. J.; Bachilo, S. M.; Huffman, C. B.; Moore, V.; Strano, M. S.; Haroz, E.; Rialon, K.; Boul, P. J.; Noon, W. H.; Kittrell, C.; Ma, J.; Hauge, R. H.; Weisman, R. B.; Smalley, R. E. *Science* **2002**, *297*, 593–596.
(43) Bachilo, S. M.; Balzano, L.; Herrera, J. E.; Pompeo, F.; Resasco, D. E.; Weisman, R. B. *J. Am. Chem. Soc.* **2003**, *125*, 11186–11187.
(44) Gomez-Gualdron, D. A.; Balbuena, P. B. *Nanotechnology* **2008**, *19*, 485604 (1−7).
(45) Lolli, G.; Zhang, L. A.; Balzano, L.; Sakulchaicharoen, N.; Tan, Y. Q.; Resasco, D. E. *J. Phys. Chem. B* **2006**, *110*, 2108–2115.
(46) Krupke, R.; Hennrich, F.; von Lohneysen, H.; Kappes, M. M. *Science* **2003**, *301*, 344–347.
(47) Arepalli, S.; Holmes, W. A.; Nikolaev, P.; Hadjiev, V. G.; Scott, C. D. *J. Nanosci. Nanotechnol.* **2004**, *4*, 762–773.
(48) Arepalli, S.; Scott, C. D. *Chem. Phys. Lett.* **1999**, *302*, 193.
(49) Arepalli, S.; Nikolaev, P.; Holmes, W. A.; Scott, C. D. *Appl. Phys. A* **2000**, *70*, 125.
(50) Arepalli, S. *J. Nanosci. Nanotechnol.* **2004**, *4*, 317.
(51) Nikolaev, P.; Holmes, W. A.; Sosa, E.; Boul, P.; Arepalli, S.; Yowell, L. *J. Nanosci. Nanotechnol.*, in press.

NL9014342